Observation of $e^+e^- \to \chi_{c1}$ at BESIII

Max Lellmann[1,*] on behalf of the BESIII collaboration

[1]Institut für Kernphysik, Johannes Gutenberg-Universität Mainz

Abstract. In electron-positron annihilation, the process of $e^+e^- \to \chi_{c1}$ can occur via the production of two virtual photons or through neutral current, therefore being suppressed with respect to the normal annihilation process via one virtual photon. Using a dedicated scan sample around the χ_{c1} mass, the direct production of χ_{c1} has been established for the first time in experiments. This provides a new approach for the study of the internal nature of hadrons.

1 Introduction

Until now, only the production of vector resonances ($J^{PC} = 1^{--}$) has been observed in e^+e^- annihilation. They are produced by the transition of a single virtual photon into a hadronic state. Particles with different quantum numbers appear in the decay of said vectors. The production of resonances with a different quantum numbers, such as axial vector states ($J^{PC} = 1^{++}$), is possible by the exchange of two virtual photons, but has not been observed yet. In the charmonium region, an obvious candidate for the search of direct production in e^+e^- collisions is the χ_{c1}. The production rate is proportional to the electronic width of the χ_{c1}. First predictions are available since the 1970s [1, 2]. Using the unitarity limit, the lower limit of the electronic width of χ_{c1} has been determined to be $\Gamma_{ee} > 0.044\,\text{eV}$, while the Vector Dominance Model suggest a width of $\Gamma_{ee} = 0.46\,\text{eV}$ [2]. There are also revisited predictions using the Vector Dominance Model [3] and calculations in non-relativistic QCD [4], which both estimate the electronic width to be in the order of 0.1 eV.

Based on the strategy of Refs. [1, 2], the authors of Ref. [5] studied the direct production of χ_{c1} and χ_{c2} in e^+e^- including interference effects between the decay of the final state $\chi_{cJ} \to \gamma J/\psi \to \gamma\mu^+\mu^-$ and the continuum background process $e^+e^- \to \gamma\mu^+\mu^-$. They predicted a width of $\Gamma_{ee} = 0.43\,\text{eV}$. The predicted interference effect shows a strong distortion of the line shape. There is constructive interference below the peak position of the χ_{c1} and destructive interference above, while at the χ_{c1} mass itself, one expects the cross section to be compatible with the expectation for the continuum process.

The BESIII collaboration studied the direct production χ_{c1} in e^+e^- collision following the strategy suggested in Ref. [5].

2 BEPCII and BESIII

The BESIII detector [6] records symmetric e^+e^- collisions provided by the BEPCII storage ring [7] in the center-of-mass energy range from 2.0 to 4.95 GeV, with a peak luminosity of

*e-mail: lellmann@uni-mainz.de

1×10^{33} cm^{-2}s^{-1} achieved at $\sqrt{s} = 3.77$ GeV. BESIII has collected large data samples in this energy region [8]. The cylindrical core of the BESIII detector covers 93% of the full solid angle and consists of a helium-based multilayer drift chamber (MDC), a plastic scintillator time-of-flight system (TOF), and a CsI(Tl) electromagnetic calorimeter (EMC), which are all enclosed in a superconducting solenoidal magnet providing a 1.0 T magnetic field. The solenoid is supported by an octagonal flux-return yoke with resistive plate counter muon identification modules interleaved with steel. The charged-particle momentum resolution at 1 GeV/c is 0.5%, and the dE/dx resolution is 6% for electrons from Bhabha scattering. The EMC measures photon energies with a resolution of 2.5% (5%) at 1 GeV in the barrel (end cap) region. The time resolution in the TOF barrel region is 68 ps, while that in the end cap region was 110 ps. The end cap TOF system was upgraded in 2015 using multigap resistive plate chamber technology, providing a time resolution of 60 ps, which benefits the data used in this analysis [9].

3 Data Samples

In 2017, a dedicated χ_{c1} mass scan has been performed, in which a set of five data points with a total integrate luminosity of 457.8 pb^{-1} have been collected in the mass range of the χ_{c1}. Two data points, one positioned at the χ_{c1} mass and one where the interference effect is expected to be largest, come with a luminosity of ≈ 180 pb^{-1} each. One data point with small statistics is taken roughly 20 MeV below the χ_{c1} nominal mass to study the continuum background process. These processes are also studied with large statistics using data samples collected at $\sqrt{s} = 3.773$ GeV and $\sqrt{s} = 4.178$ GeV with an integrated luminosity of about 3 fb^{-1} each. The center-of-mass energies are measured using the BEMS system, the integrated luminosities are determined using Bhabha events.

4 Analysis Strategy

The χ_{c1} signal is reconstructed through its decay $\chi_{c1} \to \gamma J/\psi$ with $J/\psi \to \mu^+\mu^-$. The continuum processes $e^+e^- \to \gamma J/\psi$ and $e^+e^- \to \gamma\mu^+\mu^-$ are irreducible background contributions. The Phokhara event generator [10] is used to describe the two background processes.

Event candidates are required to have two charged tracks with zero net charge, and at least one photon detected within the detector volume. A four constraint kinematic fit is performed to constrain the total final state four-momentum to the initial state four vector. If there is more than one photon in the final state, the candidate that results in the smallets χ^2 is chosen. Background from Bhabha is rejected by requiring the energy deposition of charged tracks in the calorimeter to be smaller than 0.4 GeV. The initial state radiation contribution is suppressed by requiring $|\cos\theta_\gamma| < 0.8$. After the selection, the background ratio is smaller than 1 % and only the irreducible background remains.

The samples at $\sqrt{s} = 3.773$ GeV and $\sqrt{s} = 4.178$ GeV are used to study the Monte Carlo description of the irreducible background in detail and to develop a scaling factor to compensate Data-Monte Carlo discrepancies.

After applying the correction factor to the Monte Carlo samples, discrepancies between data and Monte Carlo prediction around the J/ψ peak are studied for the four data point close to the χ_{c1} mass.

In order to extract the number of signal events at the four χ_{c1} scan points, the $M_{\mu^+\mu^-}$ and $|\cos\theta_\mu|$ spectrum is fitted using an unbinned maximum likelihood fit. The line shapes for the contributions from χ_{c1} production, irreducible background, and the interference between them are taken from Monte Carlo. The number of χ_{c1} ($N_{\chi_{c1}}$) and the number of background

events ($N_{\rm bg}$) are free parameters in the fit, while the contribution from interference is fixed to $N_{\rm int} = f \cdot \sqrt{N_{\chi_{c1}} N_{\rm bg}}$, where f is determined from a signal Monte Carlo sample, where Γ_{ee} and ϕ are set to the optimal values.

The parameters can be determined from a fit to all four data points. It is difficult to obtain an analytical formula for the cross-section of $e^+e^- \to \gamma\mu^+\mu^-$ in dependence on Γ_{ee} and ϕ. Therefore, the optimal values are determined using the scan method.

5 Results

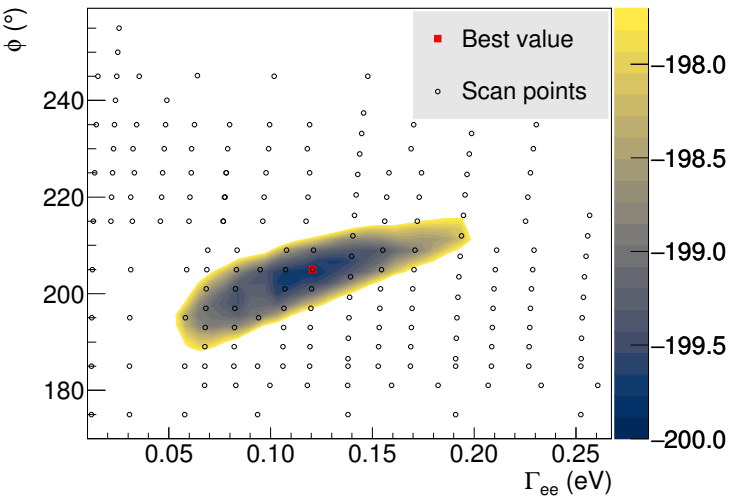

Figure 1. The 68.3 % C.L. contour of Γ_{ee} and ϕ on a distribution of log-likelihood ($-\ln L$) values. The distribution of $-\ln L$ in a larger parameter space region is shown in Supplemental Material of Ref. [11].

Figure 1 shows the scan points used to determine Γ_{ee} and ϕ in the vicinity of the best scan point, together with the 68.3 % confidence interval. The best values found are $\Gamma_{ee} = (0.12^{+0.08}_{-0.07})$ eV and $\phi = (205^{+10}_{-17})^\circ$. The given uncertainties are statistical. Using these parameters to fix f, the number of signal events $N_{\rm sig} = N_{\chi_{c1}} + N_{int}$ is found to be 210±52 at $\sqrt{s} = 3.5080$ GeV, 63±24 at $\sqrt{s} = 3.097$ GeV, 0^{+16}_{-19}, and -42±22 at $\sqrt{s} = 3.514$ GeV. The combined statistical significance, obtained by adding the log-likelihoods from each data samples, is 5.3σ. The signal cross-section is calculated from as $\sigma_{\rm sig} = \sigma_{\chi_{c1}} + \sigma_{\rm int} = N_{\rm sig}/(\varepsilon \cdot \mathcal{L})$, where ε is the reconstruction efficiency obtained from Signal MC simulations. The sum of $\sigma_{\rm sig}$ and the cross-section from ISR background taken from MC ist shown in Fig. 2 together with the expected theory curves, the observed curves and the expected curves if there was no interference.

The systematic uncertainties are 0.6 % from the luminosity measurement for each sample, 0.5 % from charged track reconstruction, and 0.2 % from photon reconstruction. The systematic uncertainties from the integrated luminosity measurement and detection efficiency are considered simultaneously by changing the normalization factor used in the scan fit by 1.0 %. The uncertainty from the $|\cos\theta_\gamma|$ constraint is obtained from varying the cut position. Other selection criteria show no significant effects. Additional studies are perfomed by changing the binning strategy, the MC normalization matrix, the beam energy spread, $M_{\mu^+\mu^-}$ fitting range, and the central position of the data samples energies.

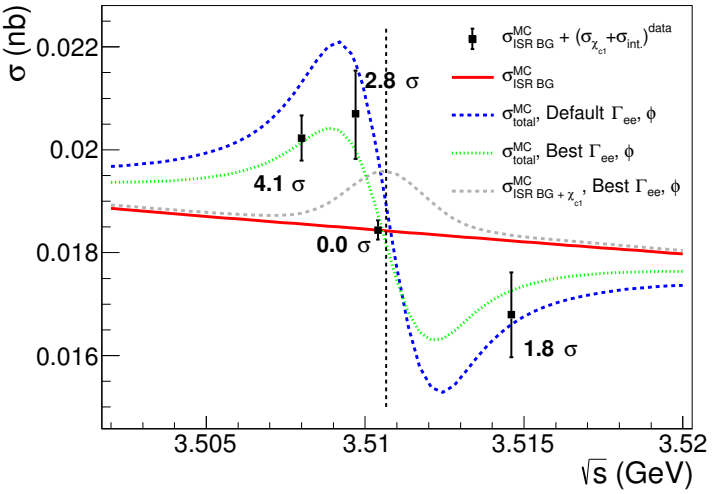

Figure 2. The colored curves are energy-dependent cross-sections of the process $e^+e^- \to \gamma J/\psi$ including (green and blue curves) and not including (red curve) the direct production of $e^+e^- \to \chi_{c1}$. The gray curve denotes the signal strength in the hypothetical case of no interference. The location of the χ_{c1} mass is indicated by the vertical line. The black dots with error bars represent $\sigma^{\rm MC}_{ISR} + \sigma^{\rm sig}$ data at the χ_{c1} scan data samples. The numbers next to the four data points indicate the statistical significances associated with the χ_{c1} production.

The obtained systematic uncertainties on Γ_{ee} and ϕ are of a similar size as their statistical uncertainty. Considering all statistical and systematic effects, the final results read $\Gamma_{ee} = (0.12^{+0.13}_{-0.08})$ eV and $\phi = (205.0^{+15.4}_{-22.4})^\circ$.

This analysis is published in Ref. [11].

References

[1] J. Kaplan and J. H. Kühn, Phys. Lett. **78B**, 2-3 (1978)
[2] J. H. Kühn, Nucl. Phys. B **157**, 125-144 (1979)
[3] A. Denig, F. K. Guo, C. Hanhart, and A. V. Nefediev, Phys. Lett. B **736**, 221-225 (2014).
[4] N. Kivel and M. Vanderhaeghen, J. High Energ. Phys. 2016:32, (2016).
[5] H. Czyż, J. H. Kühn, and S. Tracz, Phys. Rev. D **94**, 034033
[6] M. Ablikim *et al.* [BESIII Collaboration], Nucl. Instrum. Meth. A **614**, 345 (2010).
[7] C. H. Yu *et al.*, Proceedings of IPAC2016, Busan, Korea, 2016, doi:10.18429/JACoW-IPAC2016-TUYA01.
[8] M. Ablikim *et al.* [BESIII Collaboration], Chin. Phys. C **44**, 040001 (2020).
[9] X. Li *et al.*, Radiat. Detect. Technol. Methods **1**, 13 (2017); Y. X. Guo *et al.*, Radiat. Detect. Technol. Methods **1**, 15 (2017); P. Cao *et al.*, Nucl. Instrum. Meth. A **953**, 163053 (2020).
[10] H. Czyż *et al.*, Phys. Rev D **94**, 034033 (2016)
[11] M. Ablikim *et al.* [BESIII Collaboration], Phys. Rev. Lett. **129**, 122001